The Astrophysical Journal, 827:119 (9pp), 2016 August 20 doi:10.3847/0004-637X/827/2/119

SPECTRAL INTENSITIES OF ANTIPROTONS AND THE NESTED LEAKY-BOX MODEL FOR COSMIC RAYS IN THE GALAXY

R. Cowsik and T. Madziwa-Nussinov
Physics Department and McDonnell Center for the Space Sciences, Washington University, St. Louis, MO 63130, USA; cowsik@physics.wustl.edu
Received 2016 February 4; revised 2016 May 3; accepted 2016 May 21; published 2016 August 12

ABSTRACT

In this paper we note that the spectral intensities of antiprotons observed in Galactic cosmic rays in the energy range ∼1–300 GeV by BESS, PAMELA, and AMS instruments display nearly the same spectral shape as that generated by primary cosmic rays through their interaction with matter in the interstellar medium, without any significant modifications. More importantly, a constant residence time of $\sim 2.3 \pm 0.7$ million years in the Galactic volume, independent of the energy of cosmic rays, matches the observed intensities. A small additional component of secondary antiprotons in the energy range below 10 GeV, generated in cocoon-like regions surrounding the cosmic-ray sources, seems to be present. We discuss this result in the context of observations of other secondary components such as positrons and boron, and the bounds on anisotropy of cosmic rays. In the nested leaky-box model the spectral intensities of antiprotons and positrons can be interpreted as secondary products of cosmic-ray interactions.

Key words: acceleration of particles – astroparticle physics – cosmic rays – dark matter – ISM: supernova remnants

1. INTRODUCTION

The spectral intensities of antiprotons in cosmic rays provide a crucial diagnostic for understanding the origin and propagation of cosmic rays, and complement the information obtained by studying positron spectra, the ratios of secondary to primary nuclei like Li/C and B/C, and also the bounds on the anisotropy of cosmic rays. Antiproton fluxes have been measured for a long time, but it is only recently that good data over a wide energy range acquired by the PAMELA Collaboration (Adriani et al. 2009, 2010; Wu et al. 2011), the BESS Collaboration (Abe 2008), and the AMS Collaboration (Ting 2015; Ting et al. 2015) have become available. We display in Figure 1 the spectra of cosmic-ray protons, positrons, and antiprotons.

A remarkable aspect of these spectra is that beyond ∼10 GeV, protons, positrons, and antiprotons all have essentially identical spectra, $\sim E^{-2.7}$. This close similarity is indicative of their generic interconnections, and is in contrast with the spectral shape of B nuclei, displayed in Figure 2 as the B/C ratio, which falls with energy in a complex way, indicating a spectral form $\sim E^{-3.1}$ in the energy band 10–100 GeV/nucleon for B nuclei. Beyond ∼200 GeV, the experimental uncertainties increase significantly.

Traditionally, because of their very low universal abundances, Li, Be, and B have played a key role in the study of cosmic-ray propagation. Those elements have been interpreted as arising from the spallation of heavier nuclei like C, O, etc., subsequent to their acceleration to cosmic-ray energies. The decreasing B/C ratio indicates that the primary cosmic rays suffer less spallation with increasing energy up to ∼200 GeV/nucleon. The interpretation that this decrease is due to a decreasing lifetime of cosmic rays in the Galaxy faces the following difficulties. First, should such a decrease continue to much higher energies with a corresponding decrease in the leakage lifetime, then we expect the anisotropy of cosmic rays to increase continously with energy, significantly exceeding the observational bounds from a few thousand GeV onwards (Strong et al. 2007). If, in order to avoid this, one assumes that the leakage lifetime, after decreasing initially, becomes independent of energy beyond some critical energy E_c, then the spectra of the primary cosmic rays would show an upturn at this energy and have a significantly smaller spectral index at higher enegies, again contrary to observations. Thus the interpretation that the observed decrease in the B/C ratio is entirely due to spallation of primary cosmic rays in the interstellar medium is fraught with difficulties. We show a compilation of the data on anisotropies in Figure 3. In order to be consistent with the bounds on the anisotropies, the residence time of cosmic rays in the Galaxy should be at least about two million years up to energies of several hundred TeV. During this time required to establish the isotropy, spallation of primary cosmic rays will produce a base level for the B/C ratio that ought to be observed at high energies. Such an expectation is observed in the spectrum of Li nuclei presented at the 2015 cosmic-ray conference (Derome 2015; Maestro 2015; Ting 2015) and it clearly shows that at energies below ∼150 GeV/nucleon the spectrum of Li nuclei has the form $\sim E^{-3.1}$, while at higher energies it changes to $\sim E^{-2.7}$, exactly like that for all primary cosmic rays. It is not possible to interpret this behavior of the spectrum of the Li nuclei as arising from an initial decrease in the leakage lifetime of cosmic rays with energy, followed by a leveling-off to a constant lifetime at higher energies: under such circumstances we would expect the primary cosmic rays to display a change in their spectra from $\sim E^{-2.7}$ to $\sim E^{-2.4}$ at the same energy ∼150 GeV, contrary to observations. Accordingly, the interpretation of e^+, $\bar{p}$, and B all as secondary particles generated exclusively in the interstellar medium through collisions of cosmic rays is faced with the insurmountable difficulty of generating the excess B nuclei at low energies without generating a similar excess of e^+ or $\bar{p}$ at the same energies, because these two have been observed to have spectra similar to primary cosmic rays.

The difficulty noted above in the interpretation of the spectral intensities of e^+ and $\bar{p}$ in the context of the falling B/C ratio may be overcome by taking note of the kinematic differences in the production of these secondary particles: whereas the B nuclei emerge from the spallation reactions with

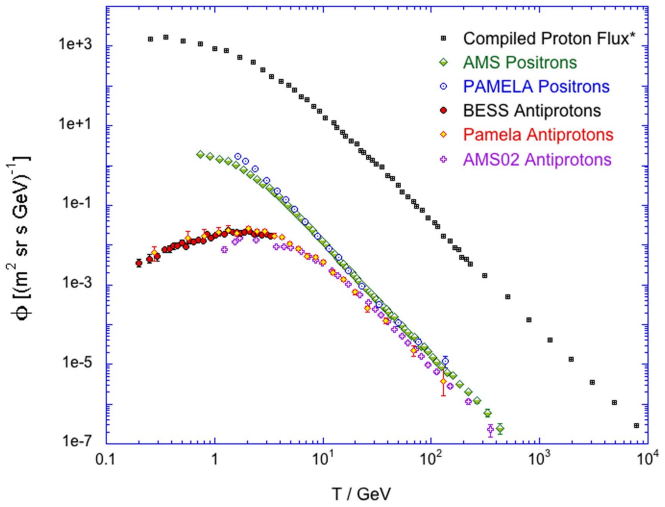

Figure 1. Experimental data on the spectral intensities of protons, positrons, and antiprotons (Abe 2008; Adriani et al. 2009, 2010, 2013; Beringer et al. 2012; Aguilar et al. 2013, 2014; Ting 2015; Ting et al. 2015). Note that all these spectra have nearly identical spectral indices at high energies, indicating a generic connection among them.

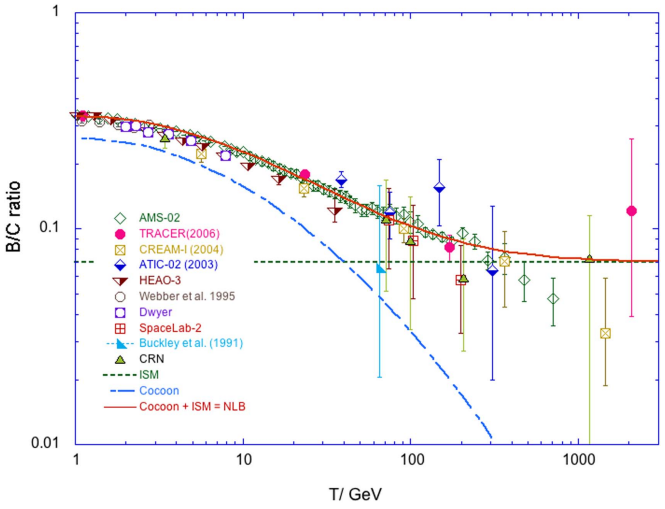

Figure 2. Observed B/C ratio is plotted along with the spectra expected from the nested leaky-box (NLB) model. The B/C data presented are taken from *HEAO*-3 (Engelmann et al. 1990), Dwyer & Meyer (1987), Chapell & Webber (1981), as well as the Tracer (Obermeier et al. 2011), *SpaceLab-2* (Müller et al. 1991), CREAM (Ahn et al. 2008), ATIC (Panov et al. 2008), Buckley et al. (1994), and AMS experiments (Oliva 2015; Ting 2015). The fit based on the NLB model is shown exclusively for the recent AMS data (Oliva 2015).

the same kinetic energy per nucleon as their parent nuclei, e^+ and $\bar{p}$ require primaries of ~20 times higher energy. In this paper, we show that within the framework of the nested leaky-box (NLB) model, these kinematic differences may be exploited to provide a consistent explanation of all three observations in a manner that satisfies the bounds on the anisotropies. Even though the NLB model was proposed long ago, it is only now, with the availability of high-quality data on e^+ and $\bar{p}$ generated by the recent experiments, that we are able to confirm its basic predictions. Indeed, Cesarsky (1980) suggested that the spectrum of antiprotons in cosmic rays would provide the crucial test for the NLB model, and the recent observations provide strong support for this model. We begin with an overview of the NLB model in Section 2. We then discuss the kinematics of the spallation and particle

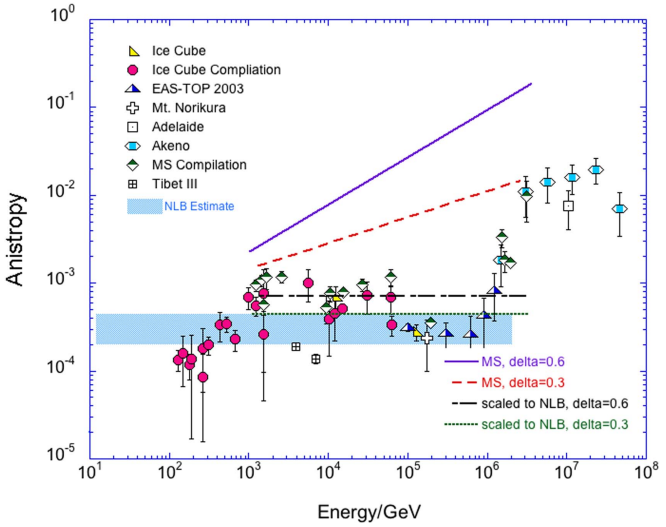

Figure 3. Measurements of the cosmic-ray anisotropy from various compilations—Strong et al. (2007), Antoni et al. (2004), Abbasi et al. (2009), Amenomori et al. (2006). Also plotted are the predictions from EDL models by Strong et al. (2007) labeled as MS and the scaled values for the NLB models from Equation (7) in Burch & Cowsik (2010). The blue shaded region shows the predicted anisotropy for the NLB model and is also from Burch & Cowsik (2010).

production processes in Section 3 and go on to calculate the expected antiproton flux in cosmic rays. In Section 4, we compare theoretical estimates with the observations. After briefly presenting alternative models for generating the antiproton flux in Section 5, we discuss the models in general, and conclude the paper in Section 6.

2. THE NLB MODEL

2.1. Earlier Developments

In the early 1970s, observational data on the composition of cosmic-ray nuclei in the energy range ~1–20 GeV/nucleon indicated that the ratios of the fluxes of secondary nuclei such as Li, Be, and B to those of their primary progenitors like C and O were decreasing functions of energy (Juliusso et al. 1972; Smith et al. 1973). This necessitated an extension of the then prevalent leaky-box (LB) model (Cowsik et al. 1966, 1967; Shapiro & Silberberg 1970, p. 323). Accordingly, the NLB model was proposed by Cowsik & Wilson (1973, 1975a, 1975b) with the following features. (a) The Galactic volume is sprinkled with a large number of sources that accelerate all cosmic-ray nuclei to nearly identical spectra, $\sim E^{-2.7}$. (b) Subsequent to the acceleration process, cosmic rays diffuse in an energy-dependent fashion in the immediate vicinity of the sources. During this period they suffer some spallation, predominantly at lower energies, before leaking into the interstellar medium. (c) Further transport of cosmic rays in the interstellar medium and the leakage from the Galaxy are energy-independent. They pointed out that with the choice for the leakage lifetime from the Galaxy, $\tau_G \sim 2$ million years, this model predicts an anisotropy that does not increase with increasing energy, and is consistent with the observational limits (Speller et al. 1972); a recent compilation of the bounds is displayed in Figure 3. Cowsik & Wilson also suggested that an explicit way to test the constancy of τ_G is that the positron spectrum in the region of ~10 GeV should have the same spectral slope as the protons at ~200 GeV. At such high

energies, protons escape readily from sources so that most positrons would be generated in interstellar space and the expectations of the NLB model are borne out (Burch & Cowsik 2010; Cowsik & Burch 2010; Cowsik et al. 2014).

This expectation is to be contrasted with models in which τ_G is assumed to be energy-dependent and which predict a steep spectrum for the positrons. This expectation of the NLB model that the positron spectrum and the proton spectrum should have similar shapes at energies in the range ~3 to ~200 GeV has been confirmed by observations by the PAMELA and AMS instruments (Adriani et al. 2009, 2010; Casaus 2009; Aguilar et al. 2014; Ting 2015). For a comparison of the spectra of e^+ and protons, see Figure 1. In her extensive review of the models of cosmic-ray propagation, Cesarsky (1980) remarked that the antiproton data provide a better test for distinguishing between the NLB and LB models, with *energy-dependent* leakage from the Galaxy suggested by Lachieze-Rey & Cesarsky (1975). In recent years this latter model has been cast in terms of cosmic-ray diffusion in a cylindrical volume and has been made more detailed by incorporating various astronomical observations of the Milky Way (Strong & Moskalenko 1998; Strong et al. 2007; Trotta et al. 2011); we refer to such models collectively as energy-dependent LB (EDLB) models. Before we estimate the antiproton spectrum, we elaborate on the basic assumptions of the NLB model.

2.2. Basic Assumptions of the NLB Model

1. Cosmic-ray nuclei are accelerated in a large number of discrete sources, which are born randomly across the Galactic disk typically once in T_b years, and inject cosmic rays into the Galactic volume for a period of about T_d years at an average rate

$$q(E) = q_0\, E^{-p} \tag{1}$$

with $p \sim 2.7$. In the present analysis of the spectral intensities of antiprotons we neglect the temporal discreteness of the sources, and assume an average number of sources. For example, if we choose $T_b \sim 50$ yr, corresponding to the supernova rate in the Galaxy, and $T_d \sim 10^5$ yr, corresponding to the oldest supernova remnants that are observed, then at any given time we have $N_s \sim T_d/T_b \approx 2000$ sources. The mean number density of sources is then given by $n_s \approx N_s/V_G$, where V_G is the volume of the cosmic-ray disc.

2. We assume that each of these sources is surrounded by a clumpy shell of stellar debris and other material, which we term the cocoon. Cosmic rays generated in the sources diffuse across such cocoons with increasing ease as the energy of the nuclei increases, so that the residence time of cosmic rays in the cocoon is a decreasing function of energy:

$$\tau_c(E) = \tau_0\, T^{-\zeta lnT}. \tag{2}$$

Here T is the kinetic energy per nucleon of the cosmic rays and ζ is a parameter to be chosen appropriately, as given below. This functional form for τ_s was introduced empirically by Cowsik & Burch (2010) and has found support from the shapes of the γ-ray spectra of several Galactic sources (Acero et al. 2015). During their transport across the cocoon cosmic rays suffer spallation and other nuclear interactions, more at lower energies and less at higher energies, following the energy dependence of their residence time $\tau_s(E)$. We show in Figure 2 a compilation of the observations of the B/C ratio in cosmic rays and fit these data with a functional form

$$\begin{aligned} \mathrm{B/C} &\propto \beta C n_{\mathrm{H,ISM}} \tau_G + \beta C n_{\mathrm{H,c}} \tau_c(E) \\ &\sim \lambda_G + \lambda_c(E). \end{aligned} \tag{3}$$

Here, $n_{\mathrm{H,ISM}}$ and $n_{\mathrm{H,c}}$ are the mean densities of hydrogen atoms in the interstellar medium and in the cocoon respectively and λ_G and $\lambda_c(E)$ are the corresponding grammages traversed by cosmic rays. The fit to the B/C data in Figure 2 yields $\zeta = 0.1$ (see Appendix A.2).

3. After emerging from the cocoon, cosmic rays propagate through the Galactic volume before they leak into intergalactic space with a lifetime τ_G. In the NLB model this lifetime is taken to be independent of the energies of the cosmic-ray nuclei, up to several hundred TeV.

$$\tau_G = \text{constant} \sim 2\ \text{Myr}. \tag{4}$$

4. With this choice of constant τ_G, the spectra of primary nuclei like p, He, C, O etc. will have nearly the same spectral shape in the Galactic volume as those generated by the sources, namely $\sim E^{-p}$, with $p = 2.7$ at high energies, say up to several hundred TeV. Note that these aspects of the NLB model differ from the EDLB model, which requires the source spectra to be $\sim E^{-2}$ or $E^{-2.4}$, so that with the choice $\tau_{G,EDLB} \sim E^{-\delta}$, with δ in the range 0.7–0.33, the observed spectra of cosmic rays may be reproduced, along with a B/C ratio continuously falling with energy as $E^{-\delta}$.

2.3. The Source Spectrum of Cosmic Rays

The importance of plane-parallel shocks as cosmic-ray accelerators was clearly brought out in the pioneering work by Bell (1978) and by Blandford & Ostriker (1978), and subsequently the rapid development of the field until the present date has been expounded elegantly in the review by Blasi (2013). The well-established result is that shocks of high Mach number accelerate cosmic rays to a spectrum of the form $\sim p^{-4}$ in 3D phase space, or equivalently $p^{-2} \sim E^{-2}$ in energy space. This result supported the requirements of a steep fall in the lifetime of cosmic rays with increasing energy, with $\tau_{G,EDLB} \sim T^{-0.6}$ in the EDLB models (Davis et al. 2000; Lave et al. 2013). In recent years, with more data extending to higher energies, the B/C ratios have suggested a significantly shallower dependence $\sim T^{-0.3}$ for τ in EDLB models (Trotta et al. 2011), especially in the context of AMS measurements with high statistics. This latter dependence of the lifetime demands that the spectrum accelerated in the sources be steeper, $\sim E^{-2.4}$, to be compared to the requirement of the NLB model, $q(E) \sim q_0 E^{-2.7}$. Thus in either case the cosmic-ray observations demand that the injection spectrum be considerably steeper than the basic predictions of diffusive acceleration in shocks of high Mach number.

Accordingly, the current research is focused on mechanisms for generating a steeper spectrum of cosmic rays by shock acceleration: under conditions of a steady state, the spectral index of cosmic rays emerging from shocks is essentially controlled by the compression ratio across the shock, x, which is 4 for shocks of high Mach number in a gas with an adiabatic index $\gamma = 5/3$. This ratio decreases as the shock speed decreases. However, the supernova blast wave has to slow

down from ~7000 km s^{-1} to at least about 70 km s^{-1} to reduce the compression ratio sufficiently to generate the $E^{-2.4}$ spectrum. At these speeds the shell of the supernova remnant carries very little kinetic energy to contribute significantly to the generation of cosmic rays. The problem of generating the required steep spectrum from fast shocks is being addressed, and several useful suggestions have been made (Blasi et al. 2012; Ellison 2013; Bell 2015). For example, Blasi et al. have suggested that the presence of neutral atoms in the shocks allows the transfer of matter, momentum, and energy through charge-exchange processes, from the downstream region to the upstream region, reducing the compression ratio, even in the case of shocks moving with high velocities. To generate the $\sim E^{-2.4}$ spectrum needed in the EDLB model, the value of x has to be reduced from its canonical value of 4 to $x = 3.15$, and to generate the $E^{-2.7}$ spectrum needed in the NLB model, x has to be lowered to a similar value, ~2.8. Thus there are workable theoretical suggestions for generating the requisite steep spectra.

2.4. Leakage Lifetime τ_G in the Galactic Volume

In all models of cosmic-ray propagation the dependence of τ_G on energy has to conform with the choice of the source spectrum, and vice versa. From the time of its original formulation the NLB model was motivated by the need to satisfy the bounds on anisotropy, and it therefore assumed τ_G to be essentially independent of energy, or at least so weakly dependent that the ratios such as B/C observed at that time could not be explained as arising from the spallation of cosmic rays only in collisions with matter in the interstellar medium. It is this choice of constant τ_G that dictated the assumption for the source spectrum, $q(E) = q_0\ E^{-2.7}$. The constancy of τ_G, at least up to several hundred TeV, is equivalent to the constancy of the diffusion constant, which is controlled by the spectrum of density inhomogeneities in the interstellar medium. A 3D Fourier decomposition of the spectrum in wavevector space is usually fit with a power law of the form

$$F(k) = k^{-p} \tag{5}$$

where the index p is related to the more familiar index ξ for the spectral density per unit interval in k through the relation $p = \xi + 2$. For an isotropic distribution of the inhomogeneities, the rigidity dependence of the diffusion coefficient in such a medium is also a power law with an index $\delta = 2 - \xi$:

$$\kappa(R) \sim \beta_c\ R^{2-\xi} = \beta_c\ R^{4-p} \approx \beta_c\ R^{\delta} \tag{6}$$

where βc and R represent the velocity and rigidity of the particles (Lee & Jokipii 1976; Cesarsky 1980). For example the EDLB models assume δ to be in the range 0.6–0.33, corresponding to $\xi = 1.4$ to 5/3. The latter value corresponds to the Kolmogorov spectrum, and is adopted more widely. In an extensive effort, Armstrong et al. (1995) have collected and analyzed astronomical observations relevant to the power spectrum of the inhomogeneities in the interstellar medium. For an assumed mean magnetic field of ~5 μG, the wavenumbers of interest for the scattering of cosmic rays with rigidities in the range ~1−1000 GV are below $\sim 10^{-10}$ m^{-1} down to $\sim 10^{-13}$ m^{-1}. In this range the observed power spectrum of the inhomoegeneities is steeper than the Kolmogorov value and fits $F(k) = k^{-p} \sim k^{-4}$. This value $p = 4$ corresponds to $\xi = 2$, and yields $\kappa \sim R^{2-\xi} \sim R^{4-p} \sim R^0 \sim$ constant. This conclusion of an energy-independent diffusion constant is strengthened by observations of the broadening of the radio pulses from pulsars, whose frequency dependence is sensitive to the index of the spectral density; the broadening is given by $b(\nu)$:

$$b(\nu) \sim b_0\ \nu^{-\alpha} \tag{7}$$

with $\alpha = 2p/(p-2)$, for $p \leqslant 4$. For a Kolmogorov spectrum with $p = 11/3$ one gets $\alpha = 4.4$. The observations and compilations by Lewandowski et al. (2013) fit $\alpha = 4$ better, corresponding to a spectrum with index $p = 4$, slightly steeper than that for the Kolmogorov spectrum. In this context, a somewhat different analysis including additional observations by Krishnakumar et al. (2015) is also relevant. Thus the assumption that τ_G is constant in the NLB model appears to be reasonable, and is consistent with observations of the inhomogeneities of the interstellar medium.

2.5. Leakage from the Cocoon

The energy dependence of the lifetime of cosmic rays in the cocoon is obtained by fitting the observed B/C ratio (exclusively to the AMS data in this paper) after subtracting the constant value expected due to spallation in the interstellar medium. The adopted functional form as given in Equation (2) is

$$\tau_c = \tau_0\ T^{-\zeta lnT}. \tag{8}$$

The shell of stellar debris and other material constituting the cocoon is likely to be highly perturbed, with much power at low k numbers similar to that in the heliosphere. Accordingly, the log-normal distribution given above and adopted for τ_c, implying a progressively larger diffusion constant with increasing energy, may be reasonable, but for the present the functional form has to be taken as one of the assumptions of the NLB model.

3. KINEMATICS OF THE PRODUCTION OF BORON, e^+, AND $\bar{p}$ IN HIGH-ENERGY INTERACTIONS

At energies beyond ~10 GeV and up to about 200 GeV the spectra of positrons and antiprotons have a spectral index of ~2.7, identical to that of their progenitors, the primary cosmic-ray protons and other nuclei. In contrast, in the same energy region, the B/C ratio decreases with increasing energy (as noted in Figure 2), indicating that the B nuclei have steeper spectra than primary cosmic rays. These differences find a natural explanation in the NLB model in terms of the differences in the kinematics of the production of e^+, $\bar{p}$, and B. The kinematic differences allow the production of the *energy-dependent* part of the B flux to be generated in the cocoons without generating significant numbers of positrons or antiprotons in the same energy band.

3.1. Kinematics of Spallation Reactions

Rare elements like Li, Be, and B in cosmic rays are produced through spallation of heavier nuclei such as C and O in collisions with interstellar hydrogen and helium via spallation reactions like

$$C + p \rightarrow B + p + \cdots \tag{9}$$

The B nucleus that arises from such an interaction has very small transverse momentum, and carries away nearly the same kinetic energy per nucleon, T, as the progenitor C. Furthermore, for $T > 1$ GeV/nucleon the cross section for spallation is nearly independent of energy up to very high energies. Accordingly, at these energies the B/C ratio is directly proportional to the amount of matter traversed by cosmic rays (neglecting, of course, futher interactions of the secondary nuclei). It is for this reason that the B/C ratio scales as $\lambda_G + \lambda_c$ defined in Equation (3), and provides a convenient way of estimating the grammage traversed by cosmic rays.

3.2. Production of Positrons

Cosmic rays generate positrons through the sequence of producing a π^+ in high-energy interactions, with a subsequent decay chain: $\pi^+ \rightarrow \mu^+ + \nu_\mu$ followed by $\mu^+ \rightarrow e^+ + \nu_e + \bar{\nu}_\mu$. The π^+ that is produced in the high-energy interactions has a wide spectrum even for a fixed energy of the primary cosmic rays. The decay chain adds further spread and shifts the energy of the positron to lower values. There are, of course, threshold effects that play a role in the production of positrons of energies below ~1 GeV. At high energies, the positrons carry away typically about a twentieth of the energy of the primary:

$$\eta_{e^+} \equiv \left\langle \frac{T_{e^+}}{T_{\rm primary}} \right\rangle \approx 0.05. \quad (10)$$

The Feynman scaling of the cross sections for high-energy interactions implies that η_{e^+} is a constant at high energies, so that the positron spectrum at any particular energy will be proportional to the spectral intensities of the primaries at energies about 20 times higher, and will have their spectral slope at that energy. An immediate consequence of the small value of $\eta_{e^+} \sim 0.05$ is that a negligible number of high-energy positrons are produced in the cocoon, because primaries with such high energy, $T \sim 20 T_{e^+}$, readily escape from the cocoon without suffering many interactions. For example, keeping in mind the current interest in the positron spectrum at energies higher than ~10 GeV, the energy of primaries needed will be in excess of ~200 GeV. At such high energies Equation (8) yields a lifetime in the cocoon that is less than ~6% of the lifetime at low energies of ~1 GeV. Accordingly, we may neglect the contribution of interactions in the cocoon to the positron flux at high energies.

If the primary spectrum is a power law throughout the energy region of interest, then the positron spectrum will also be a power law with the same index. This equality is clearly applicable to the production of positrons in the interstellar medium by Galactic cosmic rays and is the basis for the explanation of the observed positron spectrum; the complex behavior of the positron fraction, $e^+/(e^+ + e^-)$, from 1 GeV to ~200 GeV just reflects the shape of the total electron spectrum (Cowsik & Lee 1979; Burch & Cowsik 2010; Cowsik et al. 2014). To predict the positron fraction at higher energies, we have to take into account the radiative energy losses suffered by the positrons.

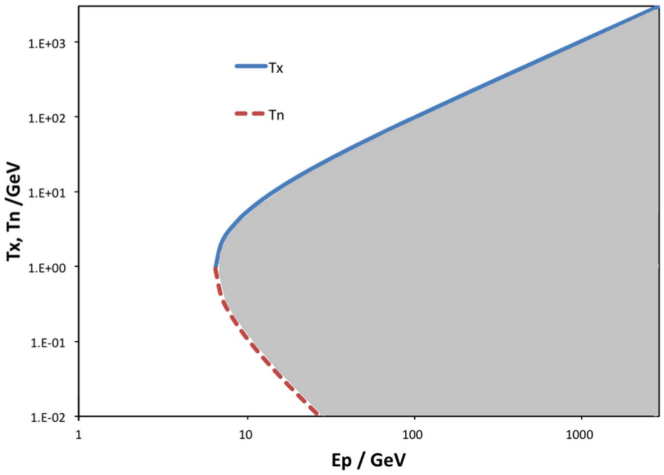

Figure 4. Kinematics of the production of antiprotons in high-energy collisions of cosmic-ray protons. Beyond the threshold at $E_p \sim 7\ m_p$, the antiproton is produced in the gray region between the maximum kinetic energy of T_x and a minimum kinetic energy of T_n, for any given energy of the primary proton.

3.3. Production of Antiprotons

Antiproton production in high-energy interactions has to be accompanied by the production of a baryon and has a threshold of $E_p = 7m_p$ in p–p collisions. Because of this the antiproton emerges from p–p collisions with a kinetic energy of $\sim m_p$ even at threshold, and as the energy of the primary increases, the spectrum of antiprotons spreads toward both lower and higher energies. We display in Figure 4 the minimum and the maximum kinetic energies, T_n and T_x, of the antiprotons generated in collisions of protons of various energies. For a primary spectrum $\sim E^{-2.7}$, we have $\eta_{\bar{p}} \approx 0.033$ at $T_{\bar{p}} = 0.1$ GeV, $\eta_{\bar{p}} \approx 0.035$ at $T_{\bar{p}} = 1$ GeV, $\eta_{\bar{p}} = 0.106$ at $T_{\bar{p}} = 10$ GeV, and $\eta_{\bar{p}} = 0.125$ for $E_{\bar{p}} = 100$ GeV and beyond. In the Appendix, we describe these kinematics in slightly greater detail and provide the details of the calculation of the antiproton fluxes, for which we have adopted the empirical fits to the cross sections in terms of the Lorentz-invariant function given by Kappl & Winkler (2014). In particular, we calculate the average value of the source function $\bar{q}_{\bar{p},c}(E)$ due to production in the cocoons and the source function $q_{\bar{p},\rm ISM}(E)$ due to the production of antiprotons in the interstellar medium.

4. COMPARISON OF THE THEORETICAL SPECTRA OF ANTIPROTONS WITH OBSERVATIONS

We have now at hand $\tau_c(E)$, or equivalently $\lambda_c(E)$, the grammage traversed by cosmic rays in the cocoons surrounding the sources, and τ_G, or λ_G, the grammage in the interstellar medium, from fitting the observed B/C ratio in cosmic rays (see Sections 2.2 and 3.1). This allows us to calculate the average rate $\bar{q}_{\bar{p},c}(E)$ at which sources inject antiprotons into unit volume of the interstellar medium; the calculation of $q_{\bar{p},\rm ISM}(E)$ is more straightforward (see Appendix A.2). These two source functions are now used to estimate the fluxes of antiprotons in Galactic cosmic rays: first we note that the contribution of the cocoons is proportional to the product of the average rate of injection of antiprotons into the interstellar medium and their effective residence time in the Galaxy before

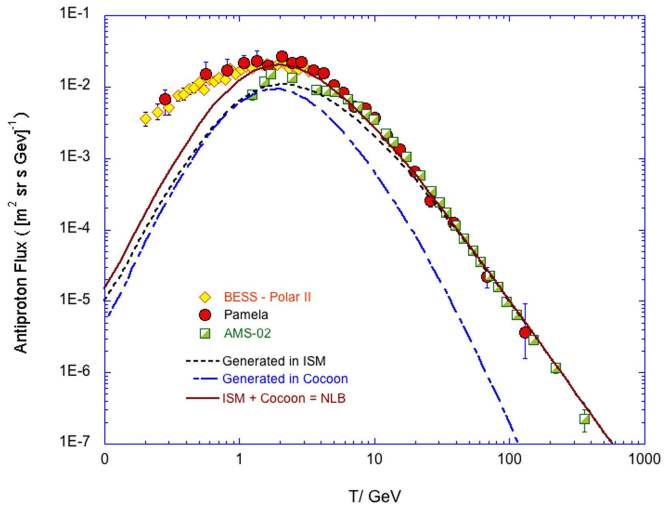

Figure 5. Spectra of antiprotons observed with the PAMELA, BESS, and AMS instruments are shown as filled dots (Adriani et al. 2010), diamonds (Abe 2008), and half-filled squares (Ting 2015; Ting et al. 2015). In this paper we have interpreted the antiproton spectrum as the sum of two components: (1) that generated in the interstellar medium (brown dashed line) where the residence time of cosmic rays is independent of their energy and (2) a small component at energies below 10 GeV, with a steep energy dependence at higher energies, generated in a cocoon-like region (blue dash-dotted line) surrounding the sources of primary cosmic rays.

leakage into intergalactic space:

$$f_{\bar{p},c}(E) = \frac{\beta c \tau_{\rm G}}{4\pi} \cdot \bar{q}_{\bar{p},c}(E). \quad (11)$$

Here βc is the velocity of the antiprotons. This contribution to the spectral intensity is displayed in Figure 5 along with a compilation of the data from BESS, PAMELA, and AMS instruments. Note that the theoretical estimate for the contributions from the cocoons is about 50% of the observed $\bar{\rm p}$ flux at ∼1 GeV and falls steeply at higher energies, as a consequence of the progressive decrease of $\tau_{\rm c}(E)$ with energy. The smaller contribution of the cocoons to the $\bar{\rm p}$ flux as compared with their contribution to the B/C ratio reflects the kinematic differences in their production—a significant contribution to the flux of $\bar{\rm p}$ at 1 GeV comes from interactions of primary protons with energies in excess of ∼20 GeV, where $\tau_{\rm c}(E)$ is much smaller than at 1 GeV.

The contribution to the $\bar{\rm p}$ flux due to the interactions of cosmic rays in the interstellar medium is given by

$$f_{\bar{p},{\rm ISM}}(E) = \frac{\beta c \tau_{\rm G}}{4\pi}\, q_{\bar{p},{\rm ISM}}(E) \quad (12)$$

and this is also displayed in Figure 5. This flux has a broader energy dependence and a spectral index ∼–2.7, similar to that of primary cosmic rays, and is the dominant contributor at high energies. The total theoretical estimate

$$f_{\bar{p}}(E) = f_{\bar{p},c}(E) + f_{\bar{p},{\rm ISM}}(E) \quad (13)$$

is also displayed in Figure 5 and provides a good fit to the observations at $E > 1$ GeV. We note that the fit below 1 GeV deviates from our estimates and can be attributed to the effects of elastic scattering of antiprotons during their propagation and adiabatic deceleration in the expanding solar wind. The remarkable similarity of the spectra of $\bar{\rm p}$ and e^+ to each other and to the primary cosmic rays provides strong support to the NLB model.

5. ALTERNATIVE MODELS AND FUTURE WORK

In the alternative scenario where scattering exclusively by Alfvén waves is postulated, the spatial diffusion is accompanied by diffusion in energy space. In fact, this diffusion in energy is evoked in all models invoking energy-dependent leakage from the Galaxy in order to fit the B/C ratio. Since all particles diffusing in the interstellar medium through scattering of Alfvén waves suffer a modification in their spectra, because of the diffusion in energy space, the injection of the primary particles should not be a power law, but one that after reacceleration is the smooth shape that is observed in Galactic cosmic rays. Furthermore, these models predict e^+ and $\bar{\rm p}$ spectra steeper than the observed spectra (which have an index of ∼2.7 at energies beyond 10 GeV) and therefore they fall below the observed intensities at high energies. Thus the alternative astrophysical or dark-matter sources of $\bar{\rm p}$ and e^+ that are invoked to account for the deficit should put out exactly such spectra, which after energy-dependent transport and reacceleration add up with the secondary component to match the observed e^+ and $\bar{\rm p}$ spectra, an unlikely coincidence. Keeping these comments in mind, we feel that the NLB model offers a plausible paradigm for understanding the observed spectra of antiprotons and positrons.

6. DISCUSSION AND CONCLUSIONS

The spectral intensities of antiprotons in cosmic rays and their ratio with respect to the intensities of their parents, mainly cosmic-ray protons, are well explained by a combination of secondary generation in the cocoons surrounding the sources and secondary generation in the interstellar medium. A crucial assumption in providing this explanation is that the leakage lifetime of cosmic rays from the Galaxy is essentially independent of energy from ∼1 GeV up to several hundred TeV, while the leakage lifetime from the cocoon decreases with increasing energy. The flatness of the observed $\bar{\rm p}/{\rm p}$ ratio at energies greater than ∼10 GeV provides strong evidence for this energy-independent residence time for cosmic rays in the Galactic volume. In our calculations we have not included any adiabatic losses due to convection or energy gains due to stochastic or other acceleration processes, or indeed any process that changes the spectral shape of the antiprotons. In this sense it is a minimal model. We have adopted this model earlier (Burch & Cowsik 2010; Cowsik et al. 2014) to interpret the B/C ratio (see Figure 2), the positron spectra (Figure 1), and the positron fraction and bounds on anisotropy of cosmic rays. The model described here is generally referred to as the NLB model for cosmic rays (Cowsik & Wilson 1973, 1975b). In this model the spectra of primary cosmic rays in the interstellar medium are essentially the same as those accelerated by the sources, and provide inputs for the choice of the source spectra used in the model calculations. Accordingly, the spectrum of γ-rays expected from the interactions of cosmic rays with interstellar matter and radiation fields is essentially a model-independent feature, and the standard interpretations of γ-ray spectra with contributions from π^0 decay and inverse-Compton scattering are valid.

However, the observed γ-ray intensities have proved useful in strengthening the ideas presented in this paper: the decay of

the neutral pions produced in high-energy interactions of cosmic rays is a major contributor to the observed γ-ray intensities, and recently Acero et al. (2016) have analyzed the data obtained from the Fermi-LAT to generate the specific emissivities of such γ-rays in the interstellar medium, as a function of galactocentric radius. As π^0 mesons are also generated in high-energy nuclear interactions of cosmic rays with interstellar matter, just like antiprotons and π^+ mesons (which yield the positrons through a decay chain), this close generic interconnection may be exploited to show that the source function for antiprotons has the correct spectral index in a broad region surrounding the solar system. The spectral emissivities in the region from ~6.5 to ~10 kpc (with the solar system located at ~8.2 kpc) have a spectral index ~2.7, the same as that assumed for primary cosmic rays for interpreting the spectra of antiprotons and positrons, in the NLB model. This is the region (with dimensions similar to the thickness of the cosmic-ray disk) from which the observed cosmic rays obtain the dominant contribution. In order to describe the cosmic-ray spectra over the whole Galaxy, the spectral variations across the disk given by Acero et al. (2016) will have to be taken into account.

The same energy-independent lifetime, τ_G, in the Galaxy and the energy-dependent lifetime, τ_c (E), in the cocoon fit all the four sets of data, namely (1) the B/C ratio, (2) the positron spectrum and the positron fraction, (3) the antiproton spectrum and the $\bar{p}/p$ ratio, and (4) the bounds on the anisotropy of cosmic rays. Here we note that the observed B/C ratios at energies beyond ~200 GeV still have uncertainties. The basic parameter, τ_G, in our model is conveniently determined by the observed Li/C and B/C ratios at these high energies. Here, the data with high statistical accuracy from the AMS instrument, which operates outside the Earth's atmosphere, where corrections due to spallation in the atmosphere are avoided, have been very useful. The data indicate a tendency for the B/C ratio to level off in the energy band 100–240 GeV/nucleon, beyond which it appears to fall again. The Li/C ratio, however, appears to level off toward a constant value in agreement with the NLB model. Additional data at energies beyond ~200 GeV/nucleon are needed to more firmly establish the behavior of the B/C ratio at high energies. Results from the CRN detector aboard the *Spacelab,* also operated outside the atmosphere, support such a leveling-off, but the statistical accuracy is very poor because of the short exposure time. An updated version of CREAM is expected to operate on the *International Space Station* and the resulting measurements will help in fixing τ_G more accurately (Seo et al. 2014). The existing data on positrons, the antiprotons, and the bounds on the anisotropy strongly suggest that τ_G is nearly constant at ~2.3 Myr up to almost $\sim 10^6$ GeV. The differences in the kinematics of their production and other factors, such as the radiative energy losses suffered by the electronic component, are responsible for the observed differences in the various ratios, even though the underlying model is the same. In conclusion, we may state that the NLB model offers a good platform for the interpretation of the fluxes of both primary and secondary cosmic rays, and is in conformity with the bounds on cosmic-ray anisotropies.

We wish to thank Professors M.H. Israel, W.R. Binns, M. A. Lee, S. Nussinov, J. Katz, and P. Blasi for extensive discussions regarding various topics in this paper. We also thank the referee (anonymous) for suggesting the importance of the γ-ray data to the modeling effort.

APPENDIX
$\bar{p}$ PRODUCTION: KINEMATICS AND SPECTRA

A.1. Some Kinematics

We present below some details of the kinematics of the production of $\bar{p}$ in $\bar{p}$–p collisions and thereafter evaluate the spectra of $\bar{p}$ generated in the cocoon and in the interstellar medium.

Consider a cosmic-ray proton of energy E_p incident on a proton at rest in the laboratory frame of reference. The velocity of the center-of-momentum frame (cms) in the lab frame is given by

$$\beta_c = p_{\rm total}/E_{\rm total} = \frac{(E_p^2 - m_p^2)^{\frac{1}{2}}}{E_p + m_p} = \left(\frac{E_p - m_p}{E_p + m_p}\right)^{\frac{1}{2}}. \quad (14)$$

Correspondingly, the Lorentz factor of the cms in the lab frame is given by

$$\gamma_c = \frac{1}{\sqrt{1-\beta_c^2}} = \left[1 - \frac{E_p - m_p}{E_p + m_p}\right]^{-\frac{1}{2}} = \left(\frac{E_P + m_p}{2m_p}\right)^{\frac{1}{2}} = \left(\frac{\gamma_l + 1}{2}\right)^{\frac{1}{2}} \quad (15)$$

where $\gamma_l = E_p/m_p$, the Lorentz factor of the cosmic-ray proton.

The total energy in the cms is generally represented by $\sqrt{s}$, where s is the Mandelstam variable; this energy is the sum of the energies of the projectile and target protons, each with an energy $\gamma_c m_p$:

$$\sqrt{s} = 2\gamma_c m_p = \sqrt{2(\gamma_l + 1)}\, m_p \quad (16)$$

or

$$s = 2(\gamma_l + 1)m_p^2 = 2(E_p + m_p)m_p. \quad (17)$$

We are interested in the maximum energy E_x^* in the cms that a $\bar{p}$ can have when produced as a $\bar{p}$–P pair. Noting that this happens when the momentum of the $\bar{p}$ balances that of three protons emerging from the collision in the cms,

$$E_x^* = \frac{s - (3m_p)^2 + m_p^2}{2\sqrt{s}} = \frac{\gamma_c^2 - 2}{\gamma_c} m_p. \quad (18)$$

Now, consider an antiproton emerging from a collision, with energy E and momentum p, at an angle θ in the lab frame. Its energy E^* is given by

$$E^* = \gamma_c(E - \beta_c p\mu) \quad (19)$$

where $\mu = \cos\theta$. The scaling variable x_R is given by

$$x_R = E^*/E_x^* = \frac{\gamma_c^2(E - \beta_c p\mu)}{m_p(\gamma_c^2 - 2)}. \quad (20)$$

The minimum value of γ_c or equivalently the minimum value of E_P, denoted as E_t, needed to generate an antiproton of energy E and momentum p is obtained by setting $x_R = 1$ and $\mu = 0$ in Equation (20) and solving for E_t. This procedure leads to a

quadratic equation for E_t:

$$aE_t^2 + bE_t + c = 0 \tag{21}$$

with the solution

$$E_t = [-b + \sqrt{(b^2 - 4ac)}]/2a \tag{22}$$

with

$$\begin{aligned} a &= 2(m_{\rm p}E - m_{\rm p}^2) \\ b &= -(2m_{\rm p}^2 + 4m_{\rm p}^2E - 6m_{\rm p}^3) \\ c &= -(2m_{\rm p}^2E^2 + 6m_{\rm p}^3E + 8m_{\rm p}^4) \end{aligned} \tag{20}$$

Equation (20) with $x_R = 1$ also defines the maximum angle θ_x or minimum value of cos θ_x at which an antiproton can be found in the lab frame in the collision of a cosmic-ray proton of energy $E_{\rm p}$

$$\theta_x = \cos^{-1}\left[\frac{\gamma_{\rm c}^2(E - m_{\rm p}) + 2m_{\rm p}}{\gamma_{\rm c}^2\beta_{cP}}\right] \tag{24}$$

which can be written in terms of $E_{\rm p}$ using Equations (14) and (15):

$$\theta_x = \cos^{-1}\left[\frac{(E_{\rm p} + m_{\rm p})(E - m_{\rm p}) + 4m_{\rm p}^2}{(E_{\rm p} + m_{\rm p})^{\frac{1}{2}}(E_{\rm p} - m_{\rm p})^{\frac{1}{2}}p}\right]. \tag{25}$$

We further note that the maximum and minimum energies of antiprotons generated in collisions of a cosmic-ray proton on a hydrogen target are given by

$$T_{x,n} = \gamma_{\rm c}(E_x^* \pm \beta_{\rm c}\sqrt{E_x^{*2} - m_{\rm p}^2}). \tag{26}$$

We show a plot of E_x and E_n as a function of E in Figure 4. Note that at high energies:

$$T_x \to E - 3m_{\rm p}, \text{ and } T_n \to m_{\rm p} \text{ as } E_{\rm p} \to \infty. \tag{27}$$

A.2. Inclusive Cross Sections for $\bar{\rm p}$ *Production and Calculation of* $\bar{\rm p}$ *Spectra*

The inclusive cross sections $d^3\sigma/d^3p$ for the production of antiprotons are generally stated in terms of the dependence of the Lorentz-invariant product $F_{p,\bar{p}} = E(d^3\sigma/d^3p)$ on the scaling variable x_R, transverse momentum $p_T = p\ \sin\theta$, etc. For the purposes of this calculation, we have made use of the empirical fits to the inclusive cross sections given by Kappl & Winkler (2014), who include the contributions of the decay of antineutrons and antihyperons to the effective cross sections. The earlier calculations of Stephens (1981), Tan & Ng (1983), Simon et al. (1998), Gaisser & Schaefer (1992), as well as the recent one of di Mauro et al. (2014) provide useful insight into the production of antiprotons by cosmic rays. We would like to rewrite this in terms of $d\sigma(E_{\rm p}, E)/dE$ for calculating the antiproton flux generated by the cosmic rays:

$$\frac{d\sigma_{\bar{p}}}{dE} = \int_0^{\theta_x}\int_0^{2\pi}\frac{F_{p\bar{p}}}{E}\,p^2\,\sin\theta\,d\theta d\varphi\,\frac{dp}{dE}. \tag{28}$$

With $p = \sqrt{E^2 - m_{\rm p}^2}$ and $dp/dE = E/p$, this becomes

$$\frac{d\sigma_{\bar{p}}}{dE} = \int_0^{\theta_x} 2\pi\,F_{p\bar{p}}\,p\,\sin\theta\,d\theta = \int_0^{\theta_x} 2\pi\,F_{p\bar{p}}\,p_t\,d\theta. \tag{29}$$

The above Equation (29) allows us to compute the source function for the antiprotons, once the spectral intensities of the cosmic-ray protons are given. To this end, let each of the sources inject cosmic-ray protons into the interstellar medium at the rate

$$q_{\rm p}(E_{\rm p}) = q_0\,E_{\rm p}^{-\beta}\ {\rm s}^{-1}\,{\rm GeV}^{-1} \tag{30}$$

where q_0 is a constant, $\beta \approx 2.7$, and $E_{\rm p}$ is in GeV. Recalling that the average number density of sources in the Galactic volume was defined as $n_s = T_d/(T_b\,V_{\rm G})$, the spectral intensity of cosmic rays in the interstellar medium becomes

$$f_{\rm p}(E_{\rm p}) = \frac{\beta\,c}{4\pi}\,n_s\,\tau_{\rm G}\,q_{\rm p}(E_{\rm p})\ {\rm cm}^{-2}\,{\rm s}^{-1}\,{\rm sr}^{-1}\,{\rm GeV}^{-1}, \tag{31}$$

where βc is the velocity of the protons. Here we have neglected the depletion of the flux of protons due to high-energy interaction because the mean free path for absorption of cosmic-ray protons is very long. The average rate at which the sources inject antiprotons into the interstellar medium is given by

$$\bar{q}_{\bar{p}{\rm c}(E)} = \int_{E_t(E)}^{\infty} X(E)\,n_s\,q_{\rm p}(E_{\rm p})\,c\,\tau_{\rm c}(E_{\rm p})\,n_{\rm H,c}\,\frac{d\sigma(E_{\rm p}E)}{dE}\,dE_{\rm p} \tag{32}$$

Here, $X(E)$ is an energy-dependent correction factor to include the contribution of He and other nuclei in the primary cosmic rays and in the target material. This was calculated by Simon et al. (1998) and parameterized by Strong & Moskalenko (1998). Also, $\tau_{\rm c}(E_{\rm p})$ is the lifetime for escape from the cocoon (see Equation (2)), $n_{\rm H,c}$ is the density of hydrogen atoms in the cocoon, and $E_t(E)$ is the threshold energy of protons needed to produce an antiproton of energy E, given in Equation (22). Note that the energy-dependent grammage in the cocoon is given by

$$\lambda_{\rm c}(E) = cn_{\rm H,c}\,\tau_{\rm c}(E)\,m_{\rm H}. \tag{33}$$

A20Similarly the source function for the production of antiprotons in the interstellar medium is given by

$$\begin{aligned} q_{\bar{p}\ {\rm ISM}}^{(E)} &= \int_{E_t(E)}^{\infty} X(E)4\pi\,f_{\rm p}(E_{\rm p})\,n_{\rm H}\,\frac{d\sigma(E_{\rm p}, E)}{dE}dE_{\rm p} \\ &= \int_{E_t(E)}^{\infty} X(E)\,n_s\,q_{\rm p}(E_{\rm p})\,\beta c\,\tau_{\rm G}\,n_{\rm H,ISM}\,\frac{d\sigma(E_{\rm p}, E)}{dE}dE_{\rm p}. \end{aligned} \tag{34}$$

Here $n_{\rm H,ISM}$ is the mean number density of hydrogen atoms in the interstellar medium and the corresponding grammage is given by

$$\lambda_{\rm G} = \beta c\,\tau_{\rm G}\,n_{\rm H}\,m_{\rm H}. \tag{35}$$

These source functions $q_{\rm p}(E_{\rm p})$, $q_{\bar{p},c}(E)$, and $q_{\bar{p},{\rm ISM}}(E)$ provide the necessary basis for the calculation of the fluxes.

Here we note that essentially the same values of the parameters determined by fitting the B/C ratio that were used in the calculations of the positron fluxes in our earlier paper (Cowsik et al. 2014) and the present set of parameters obtained by fitting exclusively the new data on the B/C ratio from the AMS instrument differ only marginally by about ~15%. Because of the uncertainties in the values of the various cross sections and because the absolute values of the various cosmic-

ray fluxes are even larger, we have at hand a consistant framework for the interpretation of the spectra and the spectral ratios of all cosmic-ray secondaries.

REFERENCES

Abbasi, R. U., Desiati, P. & for the IceCube Collaboration 2009, arXiv:0907.0498v1 [astro-ph.HE]
Abe, K. 2008, PhLB, 670, 103
Acero, F., Ackermann, M., Ajello, M., et al. 2015, ApJS, 218, 23
Acero, F., Ackermann, M., Ajello, M., et al. 2016, arXiv:1602.07246v1 [astro-ph.HE]
Adriani, O., Barbarino, G. C., Bazilevskaya, G. A., et al. (for the PAMELA Collaboration) 2009a, PhRvL, 102, 051101
Adriani, O., Barbarino, G. C., Bazilevskaya, G. A., et al. (for the PAMELA Collaboration) 2010, PhRvL, 105, 121101
Adriani, O., Barbarino, G. C., Bazilevskaya, G. A., et al. 2013, PhRvL, 111, 081102
Aguilar, M., Aisa, D., Alpat, B., et al. (for the AMS Collaboration) 2014, PhRvL, 113, 221102
Aguilar, M., Alberti, G., Alpat, B., et al. (for the AMS Collaboration) 2013, PhRvL, 110, 141102
Ahn, H. S., Allison, P. S., Bagliesi, M. G., et al. 2008, APh, 30, 133
Amenomori, M., Ayabe, S., Bi, X. J., et al. 2006, Sci, 314, 439
Antoni, T., Apel, W. D., Badea, A. F., et al. (for the KASCADE Collaboration) 2004, ApJ, 604, 687
Armstrong, J. W., Rickett, B. J., & Spangler, S. R. 1995, ApJ, 443, 209
Bell, A. R. 1978, MNRAS, 182, 147
Bell, A. R. 2015, MNRAS, 447, 2224
Beringer, J., Arguin, J. F., Barnett, R. M., et al. for Particle Data Group 2012, PhRvD, 86, 010001
Blandford, R. D., & Ostriker, J. P. 1978, ApJL, 221, L29
Blasi, P. 2009, PhRvL, 103, 051104
Blasi, P. 2013, A&ARv, 21, 70
Blasi, P., Morlino, G., Bandiera, R., et al. 2012, ApJ, 755, 121
Boyle, P., & Müller, D. 2012, PhRvD, 86, 305
Buckley, J., Dwyer, J., Muller, D., et al. 1994, ApJ, 429, 736
Burch, B., & Cowsik, R. 2010, PhRvD, 82, 023009
Casaus, J. 2009, JPhCS, 171, 012045
Cesarsky, C. J. 1980, ARA&A, 18, 289
Chapell, J. H., & Webber, W. R. 1981, Proc. ICRC (Paris), 2, 59
Cowsik, R., & Burch, B. 2010, PhRvD, 82, 023009
Cowsik, R., Burch, B., & Madziwa-Nussinov, T. 2014, ApJ, 786, 124
Cowsik, R., & Lee, M. A. 1979, ApJ, 228, 297
Cowsik, R., Pal, Y., & Tandon, S. N. 1966, PhRvL, 17, 1298
Cowsik, R., Pal, Y., Tandon, S. N., et al. 1967, PhRv, 158, 1238
Cowsik, R., & Wilson, L. W. 1973, Proc. ICRC (Denver), 1, 500
Cowsik, R., & Wilson, L. W. 1975a, Proc. ICRC (Munich), 2, 475
Cowsik, R., & Wilson, L. W. 1975b, Proc. ICRC (Munich), 2, 659
Davis, A. J., Mewaldt, R. A., Binns, W. R., et al. 2000, in AIP Conf. Proc. 528, Acceleration and Transport of Energetic Particles Observed in the Heliosphere: ACE 2000 Symp., ed. R. Mewaldt et al. (Indian Wells, CA: AIP), 421
Derome, L. Y. N. 2015, Proc. ICRC (The Hague), 589
di Mauro, M., Donato, F., Goudelis, A., et al. 2014, PhRvD, 90, 085017
Dwyer, R., & Meyer, P. 1987, ApJ, 322, 981
Ellison, D. C. 2013, AIPC, 1516, 195
Ellison, D. C., Warren, D. C., & Bykov, A. M. 2014, ApJ, 776, 46
Engelmann, J. J., Ferrando, P., Soutoul, A., et al. 1990, A&A, 233, 96
Gaisser, T. K., & Schaefer, R. K. 1992, ApJ, 394, 174
Juliusso, E., Meyer, P., & Müller, D. 1972, PhRvL, 29, 445
Kappl, R., & Winkler, M. W. 2014, JCAP, 09, 051
Krishnakumar, M. A., Mitra, D., Naidu, A., et al. 2015, arXiv:1501.05401v1 [astro-ph.HE]
Lachieze-Rey, M., & Cesarsky, C. J. 1975, Proc. ICRC (Munich), 2, 317
Lave, K. A., Wiedenbeck, M. E., Binns, W. R., et al. 2013, ApJ, 770, 117
Lee, L. C., & Jokipii, J. R. 1976, ApJ, 206, 735
Lewandowski, W., Dembska, M., Kijak, J., et al. 2013, MNRAS, 434, 69
Maestro, P. 2015, Proc. ICRC (The Hague), 1394
Müller, D., Swordy, S. P., Meyer, P., et al. 1991, ApJ, 374, 356
Obermeier, A., Ave, M., Boyle, P., et al. 2011, ApJ, 742, 14
Oliva, A. 2015, https://indico.cern.ch/event/381134/contribution/23/material/slides/0.pdf
Panov, A. D., Sokolskaya, N. V., Adams, J. H., et al. 2008, Proc. ICRC (Merida, Yucatán), 3
Seo, F. S., Anderson, T., Angelaszek, D., et al. 2014, AdSpR, 53, 1451
Shapiro, M. M., & Silberberg, R. 1970, Annual Review of Nuclear Science, Vol. 20 (Palo Alto, CA: Ann. Rev. Inc.)
Simon, M., Molnar, A., & Roesler, S. 1998, ApJ, 499, 250
Smith, L. H., Buffington, A., Smoot, G. F., et al. 1973, ApJ, 180, 987
Speller, R., Thambyapillar, T., & Elliot, H. 1972, Natur, 235, 25
Stephens, S. A. 1981, A&SS, 76, 87
Strong, A., & Moskalenko, I. 1998, ApJ, 509, 212
Strong, A. W., Moskalenko, I. V., & Ptuskin, V. S. 2007, ARNPS, 57, 285
Tan, L. C., & Ng, L. K. 1983, JPhG, 9, 227
Ting, S. 2015, Proc. ICRC (The Hague), 1376
Ting, S., et al. AMS Collaboration announcement 2015, AMS Days at CERN and Latest Results from the AMS Instrument on the International Space Station
Trotta, R., Johannesson, G., Moskalenko, I. V., et al. 2011, ApJ, 729, 106
Wu, J. & for PAMELA Collaboration 2011, ASTRA, 7, 225